



cation increases and this results from an increase in the tetragonality ( $c/a$ ) which allows increased dipolar displacements of the B-cations along the  $c$ -axis.<sup>9</sup> We also showed that this correlation of dielectric response and tetragonality could be extended to other filled TTBs, and could also be used as a simplified approximation in more complex unfilled TTB compositional series.<sup>11</sup> However, specifically for the  $\text{Ba}_6\text{MnNb}_9\text{O}_{30}$  ( $\text{M}^{3+} = \text{Ga}, \text{Sc}, \text{In}$ ) series we used a combination of temperature dependent, high resolution powder neutron diffraction and in-depth electrical characterisation to show that these materials more closely resemble dipole glass relaxors rather than relaxor ferroelectrics in nature and that the dipolar response predominantly originates from B1 displacements along the  $c$ -axis; a simple mechanism whereby the  $c$ -axis is extended by inclusion of larger B-cations allowing larger and more stable displacements explains the observed change in dielectric properties – a simple B-cation size effect.<sup>9</sup>

In this article we describe some aspects of our investigation into the effect of varying A-cation size in this structural family by systematically replacing  $\text{Ba}^{2+}$  in  $\text{Ba}_6\text{GaNb}_9\text{O}_{30}$  by the smaller  $\text{Sr}^{2+}$  and  $\text{Ca}^{2+}$  cations at the A-site. We show that a simple “average size” effect cannot be extended to this family and that instead local strain variations due to the cation size mismatch (quantified by statistical size variance) is more successful. In this respect, “average” crystal structure data obtained from traditional powder diffraction methods is not sensitive to such local variations and we show how in-depth analysis of dielectric data can be a useful tool, and also highlight some of the pit-falls and problems associated with such analysis.

## Experimental

Materials with the general formula  $\text{Ba}_{6-x-y}\text{Sr}_x\text{Ca}_y\text{GaNb}_9\text{O}_{30}$  were prepared from  $\text{BaCO}_3$ ,  $\text{SrCO}_3$ ,  $\text{CaCO}_3$ ,  $\text{Ga}_2\text{O}_3$  and  $\text{Nb}_2\text{O}_5$  (all Aldrich, 99+%) using standard solid-state methods as described elsewhere.<sup>8</sup> Stoichiometric ratios of the starting materials were ball milled and subjected to the following heating regime; 4 hours at 1000 °C, 10 hours at 1250 °C and 6 hours at 1300 °C. Phase formation was confirmed by powder X-ray diffraction (XRD) collected in transmission mode using a STOE diffractometer equipped with  $\text{Cu K}\alpha_1$  radiation (40 kV and 30 mA,  $\lambda = 1.54413$  Å) over a range of  $20 \leq 2\theta \leq 60$ . Powder neutron diffraction (PND) measurements were conducted at a constant wavelength ( $\lambda = 1.5943201$  Å) on the D2b beamline at the Institut Laue-Langevin (ILL). Neutron data were collected at room temperature with the materials loaded into 8 mm cylindrical vanadium cans. Pellets were prepared for electrical characterisation at 1300 °C and all exhibited >90% theoretical density. Pt electrodes were applied using Pt paste (Gwent Electronic Materials Ltd) and cured at 900 °C for approximately 20 minutes. Dielectric measurements were made using a Agilent 4294A impedance analyser over a frequency range of 10 Hz–13 MHz and a temperature range of approximately 20–340 K in a Sumitomo closed-cycle He cryocooler.

## Results

### Effect of average A-cation size: $\text{Ba}_{6-x-y}\text{Sr}_x\text{Ca}_y\text{GaNb}_9\text{O}_{30}$

XRD confirmed a significant phase field for formation of the TTB phase, extending to  $x = 4.5$  in the case of Sr-substitution and  $y = 3$  for Ca and  $x = 1, y = 2$  and  $x = 3, y = 2$  for co-doped compositions, Fig. 1(b). Room temperature lattice parameters were obtained by Rietveld refinement of PND data in the centrosymmetric space group  $P4/mbm$ . Full details of the refinements and refinement data are presented in the ESI.† All compounds followed Vegard’s law with a systematic decrease in both the  $ab$  and  $c$  directions, and hence volume, with decreasing average A-cation size,  $\langle r_A \rangle$ , Fig. 2 (calculations were based on 12 co-ordinate data obtained from Shannon<sup>12</sup>:  $r_{\text{Ba}} = 1.61$  Å,  $r_{\text{Sr}} = 1.44$  Å and  $r_{\text{Ca}} = 1.36$  Å).

Dielectric data showed that all compositions exhibited relaxor-like behaviour with a similar degree of frequency dispersion in the permittivity-temperature profile. Both Sr-, Ca- and Sr + Ca co-doping resulted in a displacement of the temperature of the peak maximum ( $T_m$ ) in the permittivity from that observed for the  $\text{Ba}_6\text{GaNb}_9\text{O}_{30}$  parent compound. The loss peaks were also similarly displaced. However the change in  $T_m$  does not correlate systematically with the observed changes in the unit cell parameters, *i.e.*,  $\langle r_A \rangle$ , Fig. 3(a), and hence the expected change in tetragonality as observed for the B-site substituted compounds (the isotropic contraction with decreasing average A-cation size means that the tetragonality also

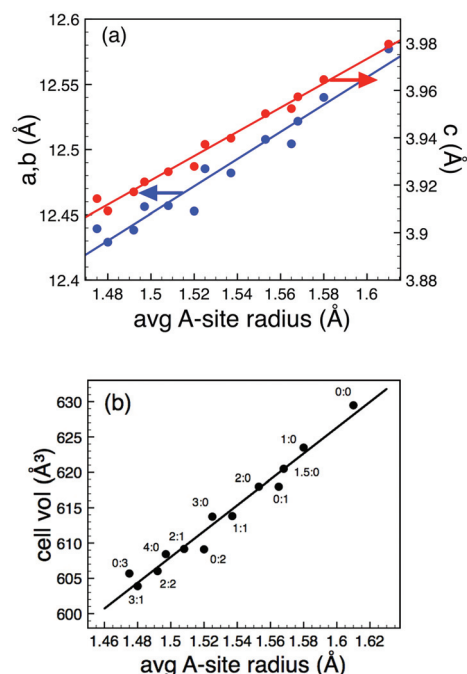


**Fig. 2** (Colour online). Lattice parameters (a) and unit cell volume (b) as a function of average A-cation size. Compositions are denoted as  $x:y$  for  $\text{Ba}_{6-x-y}\text{Sr}_x\text{Ca}_y\text{GaNb}_9\text{O}_{30}$ . Data obtained from Rietveld refinement of PND data (see ESI† for details). Note: error bars are smaller than the symbol size.



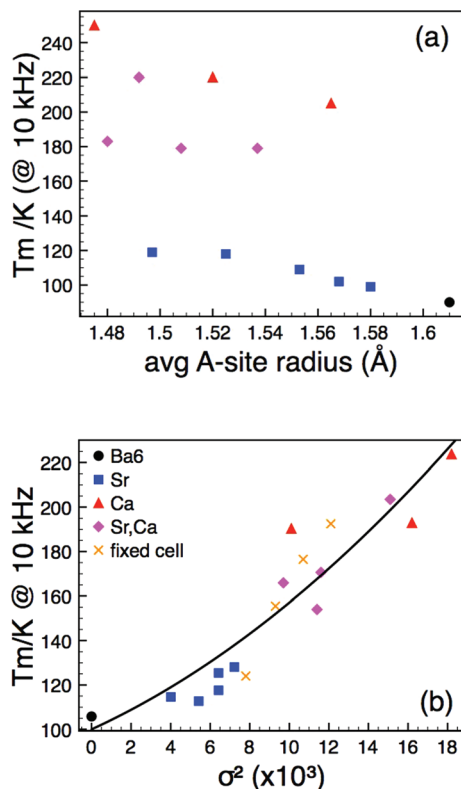


Fig. 3 (Colour online). Temperature of permittivity maxima,  $T_m$ , (measured at 10 kHz) as a function of (a) average A-cation size, and (b) A-cation size variance,  $\sigma^2$ . The solid line in (b) is a guide to the eye.

decreases monotonically with decreasing  $\langle r_A \rangle$ ). Instead  $T_m$  appears to vary systematically with the statistical A-cation size variance,  $\sigma^2$  where:

$$\sigma^2 = \langle r_A^2 \rangle - \langle r_A \rangle^2 \quad (1)$$

where  $r_A$  is the ionic radius of the cation at the A-site. Here  $\sigma^2$  simply describes the relative size distribution of cations occupying the A-site.<sup>13</sup> Whereas diffraction averages out any A-cation size differences giving a time and spatially averaged picture of the unit cell dimensions, the variance gives a quantitative measure of the degree of local disruption to be expected and hence magnitude of the “local strain” experienced by the lattice around the dopant cation point defects. First introduced by Attfield *et al.*<sup>13</sup> the size variance has been successfully used to explain the temperature dependence of magnetic phase transitions in perovskite manganites and subsequently the unusual change in the ferroelectric Curie temperature in Ca-doped BaTiO<sub>3</sub>.<sup>14</sup> It is clear that there is also a correlation with local effects (quantified by  $\sigma^2$ ) and dipole stability in these materials, Fig. 3(b). If the PND data gives the “average change” in crystal structure and  $\sigma^2$  allows some metric of local change then for the data in Fig. 3(b), both the “local” (variance) and “average” (unit cell) structure is changing – the key experiment was therefore to decouple the two.

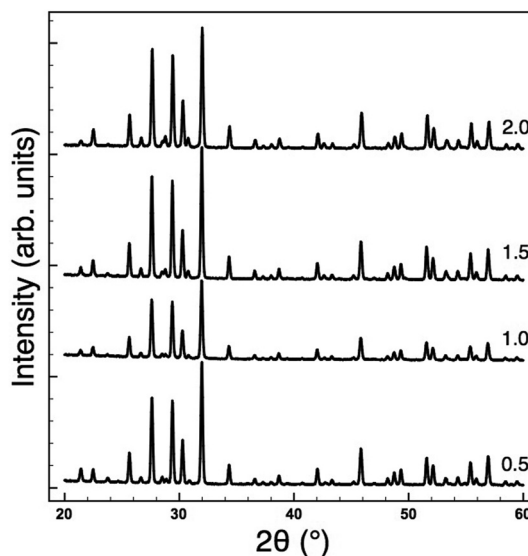


Fig. 4 XRD patterns for Ba<sub>4</sub>Sr<sub>2-z</sub>(Ba<sub>0.37</sub>Ca<sub>0.63</sub>)<sub>z</sub>GaNb<sub>9</sub>O<sub>30</sub> compositions, with z = 0.5, 1.0, 1.5 and 2.0, showing invariant lattice parameters (see Table 1).

#### Varying “local” vs. constant “average” structure

In order to decouple the two effects we adopted the approach used by Sinclair and Attfield:<sup>14</sup> starting from the Sr-doped composition Ba<sub>4</sub>Sr<sub>2</sub>GaNb<sub>9</sub>O<sub>30</sub> we systematically replaced the Sr with the appropriate ratio of larger Ba<sup>2+</sup> and smaller Ca<sup>2+</sup> ions such that their average size is equivalent to the Sr being replaced:  $r_{\text{Sr}} = 0.37r_{\text{Ba}} + 0.63r_{\text{Ca}} = 1.44 \text{ \AA}$ . This doping mechanism can be described by the general formula Ba<sub>4</sub>Sr<sub>2-z</sub>(Ba<sub>0.37</sub>Ca<sub>0.63</sub>)<sub>z</sub>GaNb<sub>9</sub>O<sub>30</sub> and allows a series of compositions to be prepared with a constant overall  $\langle r_A \rangle = 1.55 \text{ \AA}$ , but with varying size variance,  $\sigma^2$ . Four TTB compositions with z = 0.5, 1.0, 1.5 and 2.0 were prepared and their XRD patterns are shown in Fig. 4. All adopt the *P4/mbm* TTB structure and basic Rietveld refinements (including only background, zero point and unit cell) were carried out to obtain lattice parameters. The data showed that, as expected, the long-range, average structure (and tetragonality) is essentially unchanged but the variance varies significantly with z, Table 1. Dielectric data indicated that all compositions exhibit relaxor behaviour, Fig. 5, and the dielectric curves displaced to higher temperature with increasing z (see ESI†). In order to more closely quantify the changes in dielectric response we used the most common approach of fitting the frequency dependence of the temperature of the

Table 1 Unit cell parameters and variance for “fixed cell” compositions with formula Ba<sub>4</sub>Sr<sub>2-z</sub>(Ba<sub>0.37</sub>Ca<sub>0.63</sub>)<sub>z</sub>GaNb<sub>9</sub>O<sub>30</sub>

z	a (Å)	c (Å)	c/a	$\sigma^2 \times 10^3$ (Å <sup>2</sup> )
0.5	12.531	3.958	0.316	7.48
1.0	12.533	3.958	0.316	9.26
1.5	12.528	3.956	0.316	10.68
2.0	12.516	3.952	0.316	12.09



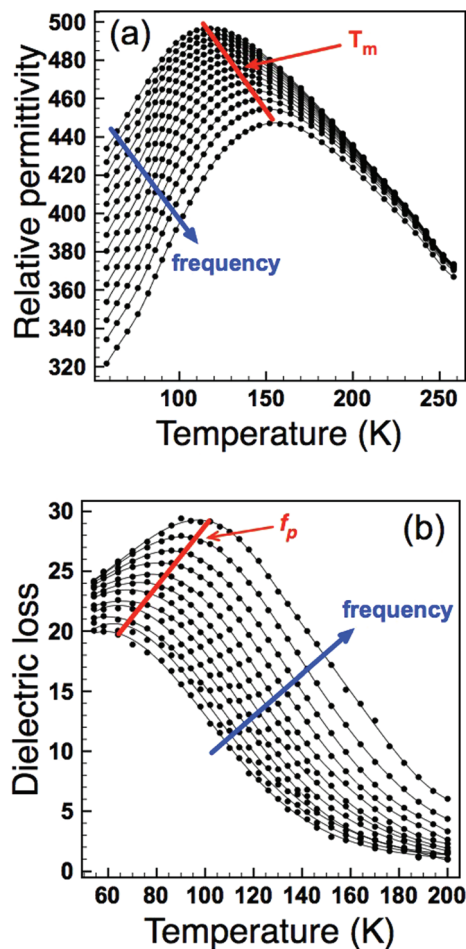


Fig. 5 Relative permittivity (a) and dielectric loss (b) as a function of frequency and temperature for  $z = 0.5$ . Temperature ( $T_m$ ) and frequency ( $f_p$ ) maxima used for dielectric analysis are indicated.

permittivity maximum,  $T_m$  according to the Vogel–Fulcher (VF) expression<sup>15</sup>:

$$f = f_0 \exp\left(-\frac{E_A}{k(T_m - T_f)}\right) \quad (2)$$

where  $f$  is the frequency of applied field,  $f_0$  is the fundamental dipole (attempt) frequency for polarisation perturbation,  $E_A$  is the activation energy associated with dipole realignment and  $T_f$  is the dipole freezing temperature. While  $T_m$  can arguably be used as a first approximation of dipole stability, and can be used for comparison among materials with similar degrees of frequency dispersion,  $T_f$  provides an “intrinsic” frequency independent parameter. Initially data were fitted with all three fitting parameters ( $f_0$ ,  $E_A$  and  $T_f$ ) unconstrained and the results presented in Table 2. The goodness-of-fit parameters suggest the VF model is a good representation of the dielectric response, with the fits shown in Fig. 6, however, there was no systematic trend in  $T_f$  or  $E_A$  with  $z$ ; the values of  $f_0$  vary far more widely than would be expected for such a structurally similar series and, more importantly, in some cases are physi-

Table 2 Calculated values for  $f_0$ ,  $E_A$  and  $T_f$  from the four different Vogel–Fulcher fitting methods employed for  $\text{Ba}_4\text{Sr}_{2-z}(\text{Ba}_{0.37}\text{Ca}_{0.63})_z\text{-GaNb}_5\text{O}_{30}$  samples

Method	$z$	$f_0$ (Hz)	$E_A$ (eV)	$T_f$ (K)	RMSD	$\chi^2$
Unconstrained	0.5	$8.42 \times 10^{11}$	0.108	55.1	0.064	0.058
	1.0	$4.84 \times 10^{17}$	0.404	7.16	0.039	0.021
	1.5	$2.41 \times 10^{16}$	0.309	50.2	0.040	0.023
	2.0	$1.55 \times 10^{16}$	0.293	71.0	0.091	0.116
Constrained $f_0$	0.5	$8.42 \times 10^{11}$	0.108	55.1	0.064	0.058
	1.0	$8.42 \times 10^{11}$	0.122	77.9	0.136	0.261
	1.5	$8.42 \times 10^{11}$	0.116	102	0.122	0.207
	2.0	$8.42 \times 10^{11}$	0.114	120	0.150	0.315
Constrained $T_f$	0.5	$7.03 \times 10^{11}$	0.105	56.0	0.064	0.058
	1.0	$4.93 \times 10^{11}$	0.114	81.4	0.147	0.302
	1.5	$3.17 \times 10^{12}$	0.135	96.0	0.102	0.145
	2.0	$2.65 \times 10^{11}$	0.097	126	0.171	0.408
Constrained $E_A$	0.5	$7.20 \times 10^{10}$	0.077	66.8	0.086	0.103
	1.0	$2.46 \times 10^{12}$	0.139	72.6	0.120	0.200
	1.5	$1.36 \times 10^{13}$	0.159	88.4	0.082	0.095
	2.0	$2.50 \times 10^{15}$	0.253	80.2	0.092	0.119

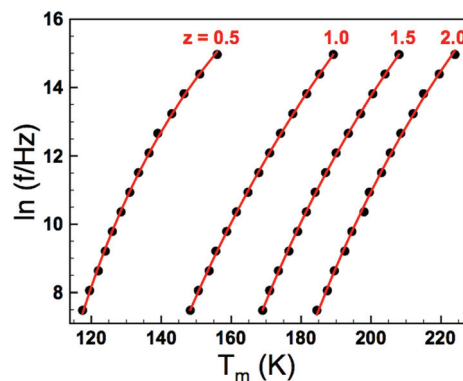


Fig. 6 (Colour online) Vogel–Fulcher fits to  $T_m(f)$  data obtained from relative permittivity profiles as shown in Fig. 5(a).

cally unrealistic for the process they describe (dipolar relaxation frequencies should be of the order  $10^9$ – $10^{12}$  Hz).

The uncertainty over the reliability of the values calculated from the unconstrained VF fits suggested that it might be desirable to re-fit the curves using a restricted, and physically realistic, value for  $f_0$ . The unconstrained fit to the data for the  $x = 0.5$  sample gave a physically realistic value for  $f_0$  of  $8.42 \times 10^{11}$  Hz and this was constrained as the value in subsequent fits for the other three compositions. Visually there was no apparent deterioration of these ‘constrained’ fits but predictably they did not have such low error analyses (Table 2) as the unconstrained fits. However, they did give physically realistic values for both  $E_A$  and  $T_f$  for all samples: the values for  $E_A$  were within those expected for dipolar processes (of the order of 0.1 eV) and the values of  $T_f$  increased systematically with increasing  $x$  – as was the expectation from visual inspection of the VF curves, Fig. 6. We have previously discussed the inherent sensitivity of VF fits to minor scatter in data points<sup>16</sup> and given that the chosen  $f_0$  value was rather arbitrary (being merely the first realistic value obtained by the unconstrained fit method) this outcome was rather unsatisfying.



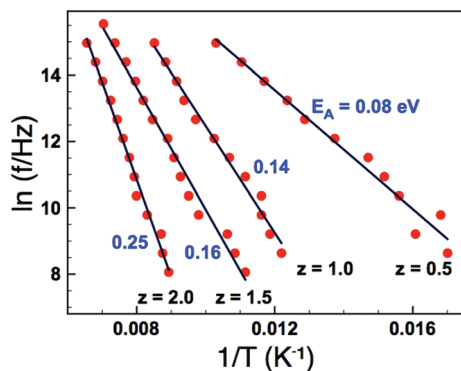


Fig. 7 (Colour online) Arrhenius plots of peak frequency ( $f_p$ ) data obtained from dielectric loss data (as shown in Fig. 5(b)).

As an alternative we analysed the dielectric loss data according to Jonscher's universal dielectric relaxation (UDR) model<sup>17</sup> to determine  $E_A$  and  $T_f$ . We have already shown this to be an effective methodology for modelling dielectric relaxation in these materials<sup>9</sup> – the parameters obtained can then be fed back into the VF analysis in order to further investigate the suitability of the VF fitting process. According to the UDR model the temperature dependence of the peak frequency,  $f_p$  in the dielectric loss, Fig. 5(b), should follow an Arrhenius expression:

$$f_p = A \exp\left(-\frac{E_A}{kT}\right) \quad (3)$$

and allows an alternative method to obtain  $E_A$ . Arrhenius plots of the loss data for all four samples are given in Fig. 7. In each case the data give a straight line, and activation energies calculated from a line of best fit give  $E_A$  values of 0.077, 0.139, 0.159 and 0.253 eV for  $z = 0.5, 1.0, 1.5$ , and  $2.0$ , respectively (Table 2). These values are all of the expected magnitude for a dipole relaxation process (as for the VF analysis), however, they show a systematic increase with increasing  $z$ . The dipole freezing temperature,  $T_f$ , can also be determined by analysis of the dielectric loss ( $\epsilon''$ ) data in the time (frequency) domain. The empirical UDR model allows fitting of a dielectric loss peak as a function of frequency according to:

$$\epsilon''(f) \propto \frac{1}{(f/f_p)^{-m} + (f/f_p)^{1-n}} \quad (4)$$

where  $f$  is the frequency of applied field,  $f_p$  is the frequency of the peak maximum and the exponents  $-m$  and  $1 - n$  describe the gradient of the  $\epsilon''(f)$  data below and above  $f_p$ , respectively (with the condition that  $0 \leq m, n \leq 1$ ). The UDR theory states the  $\epsilon''(f)$  peak associated with a dipole relaxation should become infinitely broad at dipole freezing, *i.e.*, the exponent  $m$  should tend to zero at  $T_f$ . Dielectric loss data as a function of frequency for the  $z = 0.5$  sample is shown in Fig. 8(a) and indicates that the gradient ( $m$ ) decreases with decreasing temperature. Extracting the exponent  $m$  from this data and extrapolating to  $m = 0$  allows an estimation of  $T_f$ . The results of such analysis are shown in Fig. 8(b) and summarized in

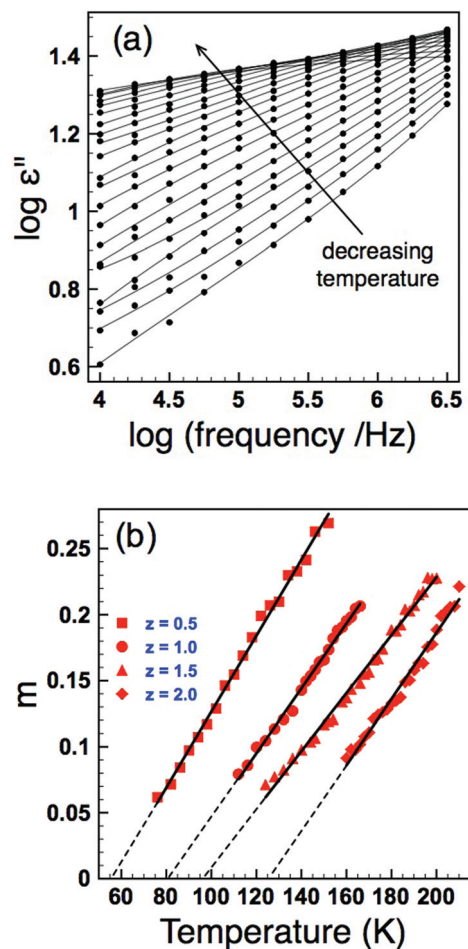


Fig. 8 (Colour online) Dielectric loss as a function of frequency showing a decrease in the frequency exponent,  $m$ , with decreasing temperature (a); determination of  $T_f$  by extrapolation of  $m$  to zero (b).

Table 2. The data clearly show a systematic increase in  $T_f$  with increasing  $z$  (increasing  $\sigma^2$ ), and furthermore the values obtained are reassuringly in reasonable agreement with those obtained for the VF fits of the real part of the permittivity when values for the fundamental frequency,  $f_0$ , were constrained to a physically sensible magnitude, Table 2.

In order to look at the self consistency of the results obtained and to highlight the variability in results obtained *via* unconstrained fitting alone, the  $E_A$  and  $T_f$  values obtained from UDR analysis of the loss data were fed back into the VF model as constrained parameters and the permittivity data fitted once more – the results are collated in Table 2. The most striking result is the consistency in results obtained *via* VF fitting where either  $f_0$  was constrained to a physically sensible limit, or where  $T_f$  had been determined from the UDR analysis of the loss data (which has demonstrated to be a robust methodology<sup>9,16</sup>); these data show a clear increase in dipole stability (quantified by  $T_f$ ) with increasing local strain (quantified by variance,  $\sigma^2$ ), Fig. 9(a). Both the unconstrained VF fits and those with  $E_A$  values obtained from UDR give no consistent trends in  $T_f$  but noticeably both also have  $f_0$  values which



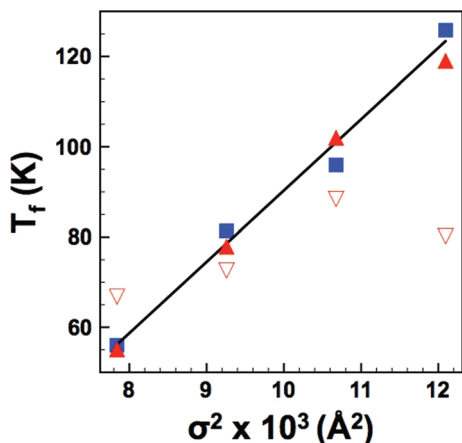


Fig. 9 (Colour online) Dipole freezing temperature,  $T_f$ , as a function of variance,  $\sigma^2$  as determined by: UDR analysis (squares); VF fits with constrained  $f_0$  (filled triangles) and constrained  $E_A$  (open triangles). Solid line is a linear fit to UDR data.

cover several orders of magnitude, a result which cannot easily be explained by such minor compositional and structural changes and which in some cases give such high frequencies as to be not physically plausible.<sup>18,19</sup> The reasons for these variations are discussed in the next section, however, considering the other results it is apparent that in the so called “fixed cell” samples with invariant average structure but increasing local variations, there is a clear and systematic change in the dielectric response as most simply evident in the displacement of the permittivity-temperature profiles (see ESI†). In depth analysis allows this relationship to be quantified in more detail as shown in Fig. 9, but it is important to link back to the original (Ba,Sr,Ca) samples which have both varying local and average structures and  $T_m$  data for the “fixed cell” samples are included for comparison in Fig. 3(b). This shows a clear relationship between dipole stability and local structural variations in these materials.

## Discussion

It is clear that VF fitting of permittivity data should be treated with caution as the parameters obtained are highly sensitive, and often give results which do not vary systematically, or which have a significant spread which cannot easily be explained by minor variations in composition and/or crystal structure. The reasons for these variations are clearly demonstrated by considering how the three fitting parameters ( $T_f$ ,  $f_0$ , and  $E_A$ ) relate to the data fits in Fig. 6(a):  $T_f$  and  $f_0$  are obtained at the limits when  $f \rightarrow 0$  and  $f \rightarrow \infty$ , *i.e.*, where the extrapolated fit tends to vertical and horizontal, respectively; the curvature of the fit is determined by  $E_A$ . Due to the combination of the degree of frequency and temperature dispersion displayed by relaxor materials and also the limited frequency range of most experimental apparatus, the  $T_m(f)$  data available for VF fitting are limited to a rather narrow range and the fit is extrapolated

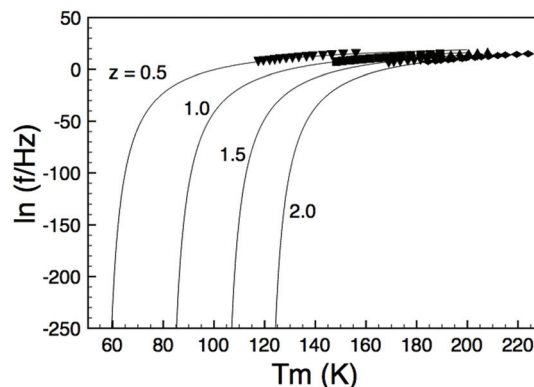


Fig. 10 Extended VF fits (with constrained  $f_0$ ) showing extrapolation for estimation of  $T_f$  as  $f \rightarrow 0$ .

over many orders of magnitude as shown by replotting the fits shown in Fig. 6(a) on an extended scale in Fig. 10. It becomes obvious therefore that even small variations in  $T_m(f)$  data (due *e.g.*, to ceramic microstructure effects) can dramatically effect the parameters obtained. In order to mitigate against this, it is expedient to either place some physically sensible restrictions on one or more parameters (*e.g.*,  $f_0$  – Table 2), or to corroborate them by alternative methods such as fitting the loss data to the UDR model. The latter approach is preferable and allows some self-consistency in the VF parameters to be evaluated. A more robust, and consistent alternative is UDR analysis of the loss data and determination of  $T_f$  by extrapolation of the  $m$  exponent of the loss peak in the frequency domain which has been shown to be consistent and relatively insensitive to ceramic microstructure.

The dielectric data show that Sr and/or Ca substitution at the A-site displaces the dielectric curves to higher temperature. The magnitude of this displacement however is not easily reconciled by a simple size effect argument. Instead the temperature dependence of the dipole stability in these relaxor materials appears to be better described by the A-cation size variance, *i.e.*, the degree of size mis-match and combined UDR analysis and restricted VF fits show that the dipole freezing temperature ( $T_f$ ) varies linearly with size variance ( $\sigma^2$ ). The effect of size variance in dipolar oxides was first studied by Sinclair and Attfield<sup>14</sup> in Sr- and Ca-doped BaTiO<sub>3</sub>. They demonstrated that while the effect of Ca-doping on the Curie temperature,  $T_C$  (which represents the dipole stability) could not be readily explained by a simple size (tolerance factor) argument, there was a clear relationship with size variance. They also reported a linear dependence with  $dT_C/d\sigma^2$  of 14 500–16 000 K Å<sup>-2</sup> compared to values of *ca.* 50 000 K Å<sup>-2</sup> for the structural transition in A<sub>2</sub>CuO<sub>4</sub> compounds and *ca.* 20 000 K Å<sup>-2</sup> for the magnetic transition in AMnO<sub>3</sub> perovskites. They attributed these differences to the differing mechanisms and suggested that *ca.* 15 000 K Å<sup>-2</sup> was the signature of a displacive (dipolar) transition. A linear fit of  $T_f$  (determined from the UDR analysis) *vs.*  $\sigma^2$ , shown in Fig. 9 gives  $dT_f/d\sigma^2 = 15\,800\text{ K Å}^{-2}$ , in excellent agreement with dipolar Ti displace-



ments in ferroelectric Ca-BaTiO<sub>3</sub>. This result is perhaps not unsurprising given that the dipolar nature of both systems arises due to B-cation displacements within the oxygen octahedra.

Sinclair and Attfield<sup>14</sup> did not describe the atomistic mechanism of dipole stabilisation, merely surmising that it was likely due to lattice strain. In a later study, Levin *et al.*<sup>20</sup> used XAFS to study the local structure in both Ca- and Sr-doped BaTiO<sub>3</sub>. Their study showed that while Sr remains centric in the A-site, Ca is displaced and this couples with the neighbouring B-site Ti displacements, stabilising it and sustaining  $T_C$ . This work has since been corroborated by the computational work of Dawson *et al.*<sup>21</sup> In simple crystallo-chemical terms this is rather easily understood: Ca is too small for the large 12-coordinate A-site of a cubic perovskite oxide and hence CaTiO<sub>3</sub> undergoes a distortion to orthorhombic *Pbnm* symmetry (the GdFeO<sub>3</sub> structure) which involves octahedral tilting to reduce the A-site volume and concomitant “anti-polar” A-site displacements in order to reduce the Ca coordination from 12 to the preferred 8. In our recent work on REScO<sub>3</sub> (RE = La, Nd, Gd) doped BaTiO<sub>3</sub> we argued that in a Ba-rich lattice the octahedral tilts are frustrated due to surrounding Ba-containing A-sites resisting this volumetric contraction, and as a result only the A-site displacement mode remains to optimise the preferred bonding environment of the smaller A-site dopant cation.<sup>22</sup> This A-site displacement couples with the B-site and stabilises  $T_C$ .

It is not immediately clear, however, why it is the statistical size variance rather than absolute size dependence (*i.e.*  $T_C$  or  $T_f$  has a root rather than reciprocal relationship with size). The work by Dawson *et al.*<sup>21</sup> suggests a delicate balance of A-site and B-site (octahedral) volume contraction and it may be coincidence that variance reflects this balance. In any case it appears that the statistical size variance allows a metric of “local structure” to be determined and which clearly has an effect on the dielectric properties. Such local information is not readily available by traditional diffraction methods and techniques which provide local structural information (such as XAFS or PDF) are required.

## Conclusions

The effect of isovalent A-site doping on the dielectric response of a family of relaxor TTBs was investigated using neutron and X-ray diffraction and in-depth analysis of dielectric data. The dielectric analysis showed that fitting of permittivity data to the widely used Vogel–Fulcher model should be treated with caution and that fitting of dielectric loss data according to the Universal Dielectric response model is a more reliable and robust method for determining the dipole freezing temperature,  $T_f$  (which is a measure of dipole stability) in these materials.

The crystallography, as determined by neutron and X-ray diffraction, indicated that all compositions obeyed Vegard’s law with unit cell metrics decreasing monotonically with

decreasing average A-cation size. In contrast the dipole stability did not vary in a similarly systematic way with A-cation size but instead  $T_f$  is directly proportional to the statistical A-cation size variance. The variance provides a measure of local structure and so it is clear that local structure plays a significant role in the dielectric response. Such information is not available *via* conventional Rietveld analysis of diffraction data and probes of local structure are required. Nevertheless, it appears that variance may be a useful metric to guide the tuning of properties in TTBs and could be extended to other structure types which contain perovskite units such as Ruddlesden-Popper and Dion-Jacobsen phases.

## Acknowledgements

The authors would like to acknowledge EaStCHEM and EPSRC (grant no. EP/F004133/1) for financial support, and Dr Clemens Ritter of the ILL for assistance in collection of neutron diffraction data.

## References

- 1 P. G. Dickens and M. S. Whittingham, *Q. Rev., Chem. Soc.*, 1968, **22**, 30.
- 2 A. Simon and J. Ravez, *C. R. Chim.*, 2006, **9**, 1268–1276.
- 3 P. B. Jamieson, S. C. Abrahams and J. L. Bernstein, *J. Chem. Phys.*, 1969, **50**, 4352.
- 4 P. Labbe, H. Leligny, B. Raveau, J. Schneck and J. C. Toledano, *J. Phys.: Condens. Matter*, 1990, **2**, 25–43.
- 5 P. B. Jamieson, S. C. Abrahams and J. L. Bernstein, *J. Chem. Phys.*, 1968, **48**, 5048.
- 6 I. Levin, M. C. Stennett, G. C. Miles, D. I. Woodward, A. R. West and I. M. Reaney, *Appl. Phys. Lett.*, 2006, **89**, 122908.
- 7 M. C. Stennett, I. M. Reaney, G. C. Miles, A. R. West, C. A. Kirk and I. Levin, *J. Appl. Phys.*, 2007, **101**, 104114.
- 8 D. C. Arnold and F. D. Morrison, *J. Mater. Chem.*, 2009, **19**, 6485–6488.
- 9 A. Rotaru, D. C. Arnold, A. Daoud-Aladine and F. D. Morrison, *Phys. Rev. B: Condens. Matter*, 2011, **83**, 184302.
- 10 A. Rotaru, A. J. Miller, D. C. Arnold and F. D. Morrison, *Philos. Trans.: Math., Phys. Eng. Sci.*, 2014, **372**, 20120451.
- 11 J. Gardner and F. D. Morrison, *Dalton Trans.*, 2014, **43**, 11687–11695.
- 12 R. D. Shannon, *Acta Crystallogr., Sect. A: Found. Crystallogr.*, 1976, **32**, 751–767.
- 13 J. P. Attfield, *Chem. Mater.*, 1998, **10**, 3239–3248.
- 14 D. C. Sinclair and J. P. Attfield, *Chem. Commun.*, 1999, 1497–1498.
- 15 D. Viehland, S. J. Jang, L. E. Cross and M. Wuttig, *J. Appl. Phys.*, 1990, **68**, 2916.
- 16 A. Rotaru and F. D. Morrison, *J. Therm. Anal. Calorim.*, 2015, DOI: 10.1007/s10973-014-4355-5.



- 17 A. K. Jonscher, *Dielectric Relaxation in solids*, Chelsea Dielectrics Press, London, 1983.
- 18 F. Bahri, H. Khemakhem, M. Gargouri, A. Simon, R. Von der Mühlh and J. Ravez, *Solid State Sci.*, 2003, **5**, 1445–1450.
- 19 H. Du, W. Zhou, F. Luo, D. Zhu, S. Qu and Z. Pei, *J. Appl. Phys.*, 2009, **105**, 124104.
- 20 I. Levin, V. Krayzman and J. C. Woicik, *Appl. Phys. Lett.*, 2013, **102**, 162906.
- 21 J. A. Dawson, D. C. Sinclair, J. H. Harding and C. L. Freeman, *Chem. Mater.*, 2014, **26**, 6104–6112.
- 22 S. A. Turp, PhD thesis, *Chemical control of the polymorphic phase boundaries in doped barium titanate*, University of St Andrews, 2013.

